

Mesoporous Carbons | Hot Paper |

Mesoporous Carbons Templated by PEO-PCL Block Copolymers as Electrode Materials for Supercapacitors**

Jheng-Guang Li,^{*[a, b]} Ya-Fan Ho,^[a] Mahmoud M. M. Ahmed,^[a] Heng-Chia Liang,^[b] and Shiao-Wei Kuo^{*[a, c]}

Abstract: In this study, samples of activated mesoporous carbon are fabricated with pore structures with cylinder and gyroid nanostructures through the templating effect of amphiphilic poly(ethylene oxide-*block*-caprolactone) (PEO-PCL) and by using specific resol/PEO-PCL weight ratios (e.g., 60:40 for cylinders; 55:45 for gyroids). After carbonization and KOH activation, the activated mesoporous carbons were tested as electrode materials for electric double-layer capacitor (EDLC) supercapacitors. The electrochemical properties were examined by using three-electrode (6 M KOH_(aq) as electrolyte) and CR2032 coin-cell (1 M tetraethylammonium tetra-

fluoroborate (TEABF₄)/CN as the electrolyte) systems. The gyroid carbon samples provided specific capacitances higher than those of the cylinder carbon samples in both aqueous and organic systems: 155 Fg⁻¹ compared with 135 Fg⁻¹ in 6 M KOH_(aq), and 105.6 compared with 96 Fg⁻¹ in 1 M TEABF₄/MeCN, after 100 charge/discharge cycles. It is suspected that the bi-continuous mesochannels of the gyroid-type activated mesoporous carbons provided a relatively higher effective adsorption surface area; in other words, the greater surface area for energy storage originated from a moderate pore size and an interconnected pore structure.

Introduction

Many studies at present are focused on electrode materials for energy storage devices, including fuel cells,^[1,2] solar cells,^[3-5] lead-acid batteries,^[6,7] lithium-ion batteries,^[8-10] and supercapacitors.^[11-14] Supercapacitors, especially those for electrochemical double-layer capacitors (EDLCs), are receiving much attention for their high power densities, environmentally friendly compositions, and high cycle life.^[15-17] The main electrode materials for EDLC supercapacitors are porous carbons, which provide large surface areas for the adsorption of cations and anions. Industrially, the most popular electrode materials are activated carbons, owing to their low cost and amenability to mass production; nevertheless, there are limitations when using the current activated carbons as electrode materials for

supercapacitors—for example, the high surface area of most activated carbons is attributed mainly to micropores, which restricts the types of electrolytes that can be applied in supercapacitors. The energy density (E) of a supercapacitor can be calculated by using the formula, $E = 1/2 CV^2$, where C is the capacitance and V is the working voltage. The energy density will be restricted if the pore sizes are distributed only in the micropore zone; accordingly, the regulation of pore sizes, or even pore structures, remains a challenge.^[18]

Several porous carbons with various morphologies or pore structures have been developed for matching with electrolytes in supercapacitors, including curled graphenes,^[19] templated carbons,^[20] hierarchical porous carbons,^[21] and others.

Mesoporous carbons templated directly by Pluronic F127 (EO₁₀₆PO₇₀EO₁₀₆), a soft template, have attracted much attention as electrode materials for supercapacitors because of their tunable mesoporous structures. These mesoporous carbons are fabricated through an organic–organic self-assembly strategy with F127 as the structure-directing agent and phenolic resin (resol or novolac) as the carbon source.^[22,23] Many amphiphilic block copolymers have been used recently as templates for the synthesis of mesoporous carbons, including PEO-PS (poly(ethylene oxide)-*block*-polystyrene),^[24] PEO-PMMA (poly(methyl methacrylate)),^[25] and PEO-PCL (poly(ethylene oxide-*block*-caprolactone)).^[26] In previous studies,^[26-30] we employed the macroinitiator of MPEO and the CL monomer to synthesize a series of amphiphilic PEO-PCL block copolymers; these lab-made templates could be tailored with various molecular weights, thereby leading to various microphase-separated structures. For this reason, PEO-PCL could be a wonderful candidate based on the flexibility of tunable pore size and pore

[a] Dr. J.-G. Li, Y.-F. Ho, Dr. M. M. M. Ahmed, Prof. S.-W. Kuo
Department of Materials and Optoelectronic Science
Center of Crystal Research, National Sun Yat-Sen University
Kaohsiung (Taiwan)
E-mail: kuosw@faculty.nsysu.edu.tw

[b] Dr. J.-G. Li, Dr. H.-C. Liang
R&D Department, Asia Carbons &
Technology Inc. Taoyuan (Taiwan)

[c] Prof. S.-W. Kuo
Department of Medicinal and Applied Chemistry
Kaohsiung Medical University
Kaohsiung 807 (Taiwan)
E-mail: kuosw@faculty.nsysu.edu.tw

[**] PEO-PCL = poly(ethylene oxide-*block*-caprolactone).

Supporting information and the ORCID identification number(s) for the author(s) of this article can be found under:
<https://doi.org/10.1002/chem.201901724>.

structures of mesoporous carbons. Moreover, the carbon source of phenolic resin could be tuned to a specific volume fraction when blended with a soft PEO-PCL template, thereby inducing various mesoporous structures after thermal removal of the template. This templating method can be a useful approach for controlling mesopore sizes and mesopore structures. In this present study, we synthesized PEO-PCL ($M_n = 15\,000\text{ g mol}^{-1}$; EO₁₁₄CL₉₂) as a soft template and combined it with resol-type phenolic resin to fabricate mesoporous carbons with hexagonal or gyroid packing pore structures. The surface areas of these carbon materials increased after applying a simple KOH activation method.^[22] By using this approach, we fabricated activated mesoporous carbons with large pore sizes (14–16 nm), specific structures (hexagonal or gyroid), and high surface areas (1800–2000 m²g⁻¹), and applied them as electrode materials in EDLC supercapacitors. We examined the electrochemical properties of these mesoporous carbons with large mesopores within three-electrode KOH_(aq) and CR2032 coin cell (1 M tetraethylammonium tetrafluoroborate (TEABF₄) in MeCN) systems. Interestingly, the organic capacitances of both types of activated mesoporous carbon electrodes were slightly lower than their corresponding aqueous capacitances; normally the organic capacitance for an activated carbon electrode is lower than the aqueous capacitance because the porosity is contributed mainly by micropores. In addition, for both organic and aqueous capacitances, the capacitances of the activated mesoporous carbons with the gyroid pore structure were higher than those of the activated mesoporous carbons with cylindrical pore structure, presumably because of the interconnected mesopores in the gyroid structure. These findings confirm that the pore structure is also an important parameter affecting ion transportation and adsorption. After activation, we obtained mesoporous carbons with two unique structures (cylinder and gyroid) and surface areas close to 2000 m²g⁻¹ (1865 and 1920 m²g⁻¹, respectively). Most surprisingly, the structures of the two activated mesoporous carbons remained intact after fine-tuning the activation conditions.

Experimental Section

PEO-PCL and resol-type phenolic resin

The PEO-PCL amphiphilic block copolymer was synthesized through ring-opening polymerization with monomethoxy poly(ethylene oxide) (PEO₁₁₄; molecular weight: 5000; Fluka) as the macroinitiator, ε-caprolactone (ε-CL, Acros) as the monomer, and stannous(II) octoate [Sn(Oct)₂, Sigma] as the catalyst. The molecular weight of PEO-PCL was designed to be approximately 15 000 g mol⁻¹.^[31] The resol was prepared through condensation of phenol, CH₂O with NaOH, producing a resol resin with an average molecular weight (M_n) of approximately 500.^[26]

Mesoporous carbons and activated mesoporous carbons

Mesoporous carbons were synthesized from resol phenolic resin as the carbon precursor and PEO-PCL as the template, with a specific weight ratio of resol to PEO-PCL (60:40 for hexagonal cylinder structures; 55:45 for gyroid structures). PEL-PCL (1 g) was dissolved in THF (20 g) and resol (corresponding weight) was dissolved in

THF (10 g). These two solutions were mixed together, poured into the Petri dishes and the solvent was evaporated for 8 h. The Petri dishes were then transferred to an oven for curing (150 °C, 24 h). The mesoporous carbons were obtained after removal of the template through calcination for 3 h under a N₂ atmosphere (at 1 °Cmin⁻¹ up to 400 °C and then at 1.6 °Cmin⁻¹ up to 700 °C). In the following activation step, the mesoporous carbons with a specific mesophase (hexagonal cylinder or gyroid) were dispersed in KOH_(aq) at 60 °C for 3 h, dried at 100 °C for 12 h, and then calcinated at 800 °C under N₂ (5 °Cmin⁻¹). The thermally treated samples were neutralized with 2 M HCl_(aq), washed with de-ionized water, and dried in an oven at 70 °C for 12 h.

Characterization

Small-angle X-ray scattering (SAXS) was performed by using the SWAXS instrument at the BL17B3 beamline [wavelength (λ): 1.24 Å] at the NSRRC, Taiwan. The d -spacings of mesoporous structures were calculated by using the Bragg diffraction formula. Transmission electron microscopy (TEM) images were recorded by using a JEOL 2100 microscope operated at 200 kV; the samples for TEM analyses were suspended in EtOH and then supported onto the holey carbon film on the Cu grid. Nitrogen adsorption/desorption isotherms were recorded at -196 °C, by using an ASAP 2020 analyzer; the mesoporous materials were degassed under vacuum at 200 °C for 6 h prior to measurement. The Brunauer–Emmett–Teller (BET) method was used to measure the specific surface areas and pore volumes; the pore size distributions were derived from the adsorption branches of the isotherms, based on the Barrett–Joyner–Halenda (BJH) model. Raman spectra were measured at room temperature by using a Jobin–Yvon T6400 micro-Raman system, with the 325-nm line of a He–Cd laser as the excitation source.

Electrochemical measurements

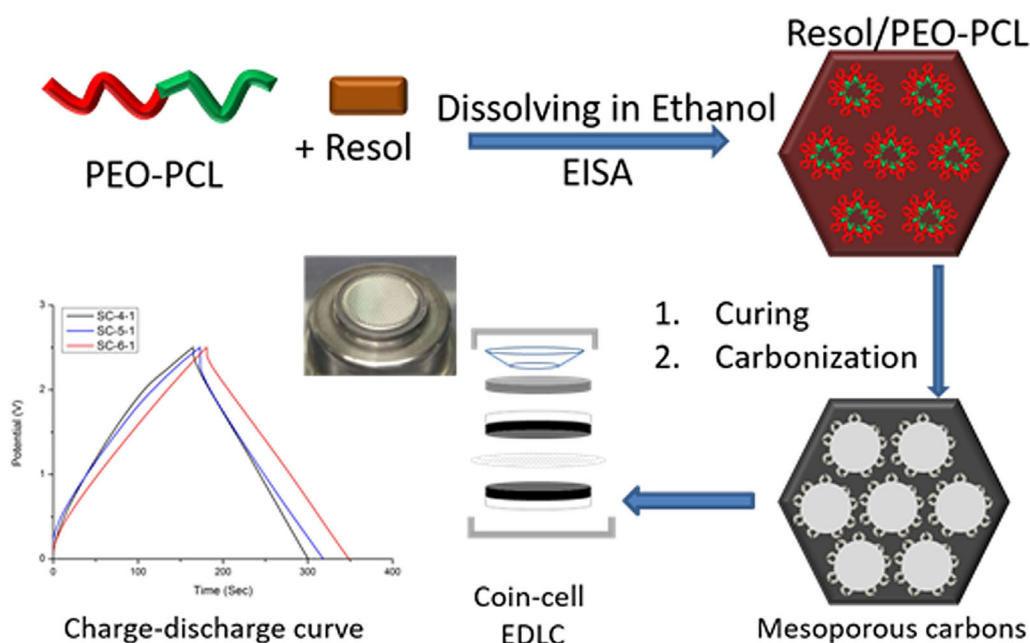
The electrochemical properties of the activated mesoporous carbon samples as electrode materials for EDLC supercapacitors were determined by using a three-electrode system (6 M KOH_(aq)) and a two-electrode system (1 M TEABF₄/MeCN in a coin-cell). To prepare the working electrode for the three-electrode system, 80 wt% of the active material (porous carbon), 10 wt% acetylene black, and 10 wt% polytetrafluoroethylene (PTFE) were dispersed in EtOH, dried in an oven at 80 °C, and then pressed onto nickel foam at a pressure of 50 kgfcm⁻² for 3 min. The prepared electrodes were placed in an oven at 100 °C until required for electrochemical tests. The working electrodes were characterized through cyclic voltammetry (CV) at a scan rate of 5 mVs⁻¹ and through charge/discharge tests at a specific static current density (0.5, 1, 2, 3, or 5 Ag⁻¹); these experiments were performed in a Metrohm Autolab PGSTAT204 system by using Ag/AgCl as the reference electrode and Pt as the counter electrode. The activated mesoporous carbon samples were also tested as electrode materials for EDLC supercapacitors in CR2032 coin-type cells. The electrodes were fabricated by mixing 80 wt% of the active material (porous carbon), 10 wt% acetylene black, and 10 wt% PTFE to form a homogeneous slurry, which was transferred to Al foil, cut into round shapes, and used in the assembly of CR2032 EDLC supercapacitors. The coin-cell supercapacitors were assembled in a glovebox under an Ar atmosphere, in the order: bottom, electrode, separator (with electrolyte), electrode, spacer, springs, and cap. The electrochemical performances of the active materials were tested through galvanostatic charge/discharge measurements at a current density of

1.0 Ag⁻¹ (voltage window: 0–2.5 V) by using an AcuTech BAT-750B battery tester.

Results and Discussion

To fabricate the mesoporous carbons, we first synthesized an amphiphilic PEO-PCL block copolymer with specific molecular weight fractions (EO₁₁₄-CL₉₂) as the template; in previous studies, we found that such templates are suitable for the preparation of ordered mesoporous carbons with hexagonal cylinder and gyroid structures.^[26–29] The resol-type phenolic resin and this PEO-PCL template were dissolved in EtOH at a specific weight ratio; the microphase transferred gradually to an ordered structure after evaporation-induced self-assembly and curing in the oven, with the electrode materials for EDLC supercapacitors obtained after carbonization and activation processes (Scheme 1). The weight ratios of resol to PEO-PCL could be regulated during the fabrication of the mesoporous car-

bons to induce different types of microphase separation, based on the corresponding volume fractions of the PCL and resol/PEO domains. Figure 1 presents SAXS patterns and TEM images of the mesoporous carbons, revealing how the mesophase changed with respect to the resol/PEO-PCL ratio. A gyroid structure was formed when the resol/PEO-PCL weight ratio was 55:45; the SAXS pattern displays the reflections 6^{1/2}, 22^{1/2}, 38^{1/2}, and 46^{1/2} and the TEM image features the typical (111) face of a gyroid structure. The mesophase transferred from a gyroid to a cylinder structure when the weight fraction was increased to 60:40 (Figures 1e and d); the SAXS reflection series of 1, 3^{1/2}, 2, and 7^{1/2} is typical of a hexagonal cylinder structure, whereas the TEM image (Figure 1d) presents the top view of hexagonally packed pores, consistent with the mesophase change in the two-phase diagram.^[32] The mesoporous resol or carbon was not formed, because of an incomplete resol domain, when the resol/PEO-PCL weight fraction was less than 50:50 (Figures 1f–i); in this case, the mesophase trans-



Scheme 1. Fabrication of mesoporous carbons and their application in supercapacitors.

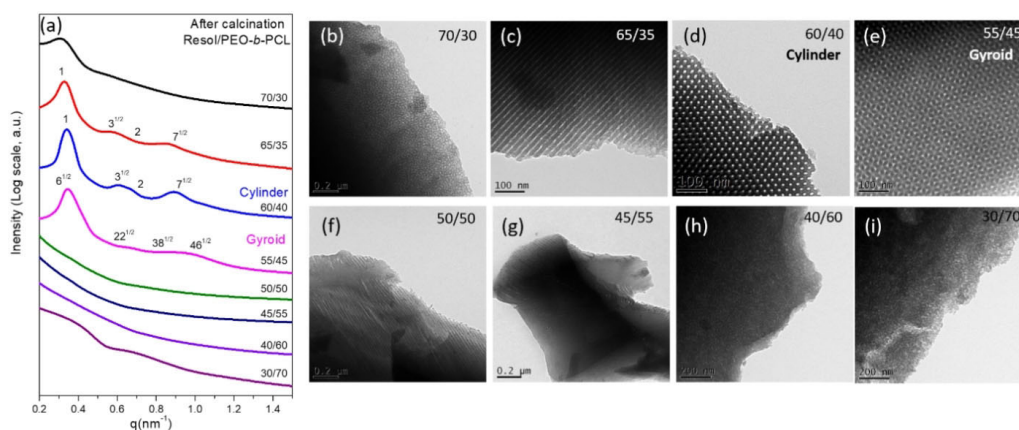


Figure 1. (a) SAXS and (b–i) TEM analyses of mesoporous carbons templated at various resol/PEO-PCL weight ratios.

formed gradually to a disordered spherical pore structure, as displayed in Figure 1 b.

We used N_2 isotherm sorption experiments to determine the surface areas, pore sizes, and pore properties of our mesoporous carbons (Figure 2, Table 1). Figure 2a presents the N_2 adsorption/desorption curves of mesoporous carbons templated

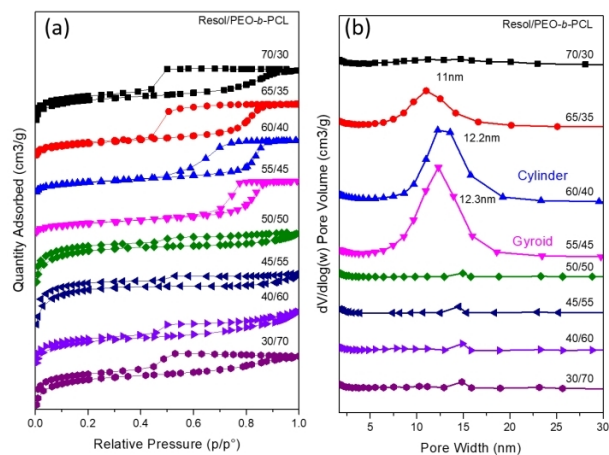


Figure 2. (a) N_2 adsorption/desorption isotherms and (b) pore size distribution curves of mesoporous carbons templated at various resol/PEO-PCL weight ratios.

by using various resol/PEO-PCL weight ratios; typical hysteresis loops are evident at all weight fractions. The hysteresis loops of the 55:45 and 60:40 samples were of H_1 type (cylindrically shaped pores), consistent with the mesophases observed in the TEM images and SAXS patterns for the gyroid and cylinder structures, respectively. When we increased the resol/PEO-PCL weight ratio to 65:35, spherical pores were observed, as evident from the H_1 -type hysteresis loops in Figure 2b. We calculated the pore size distributions of the mesoporous carbons from the adsorption branches of their hysteresis loops, based on the BJH method (Figure 2b). Interestingly, the mesoporous character was more apparent when the mesophase tended to be ordered, such as in the gyroid and hexagonal cylinder structures. The mesopores of the gyroid and cylinder structures not only had similar pore shapes but also a similar pore size of 12 nm. Table 1 lists the BET surface areas, micropore surface areas, pore volumes, and micropore volumes of our mesoporous carbon samples; these data confirmed that the ordered

structures, including cylinders and gyroids, also exhibited rich mesopore structures.

To study the suitability of using these mesoporous carbons as electrode materials for EDLC supercapacitors, we selected two types of mesoporous carbons, with specific gyroid and cylinder structures, for the following experiments (Figure 3 and Figure 4). EDLC supercapacitors store their electrical energy through a static electricity effect; hence, when using mesoporous carbons as electrode materials, the first step is their activation to provide larger surface areas for the adsorption of the electrolyte (Figures 3 and 4). Figure 3a displays the SAXS pat-

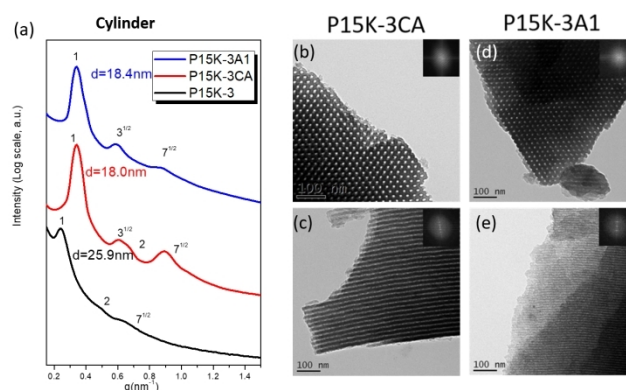


Figure 3. (a) SAXS and TEM analyses of mesoporous carbons with cylindrical structures (b, c) before (P15K-3CA) and (d, e) after (P15K-3A1) activation.

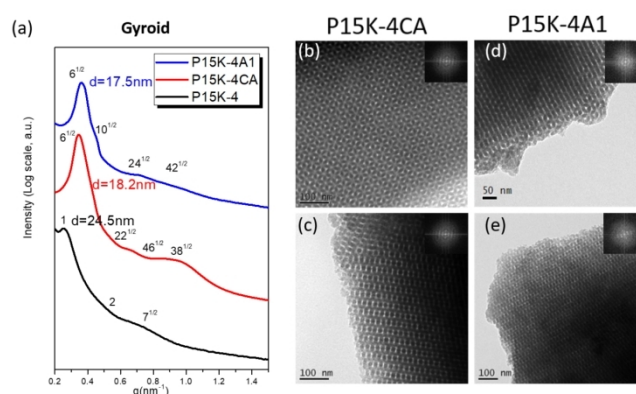


Figure 4. (a) SAXS and TEM analyses of mesoporous carbons with gyroid structures (b, c) before (P15K-4CA) and (d, e) after (P15K-4A1) activation.

Sample	Resol/PEO- <i>b</i> -PCL	S_{BET} [m ² g ⁻¹] ^[a]	S_M [m ² g ⁻¹] ^[a]	V_{total} [cm ³ g ⁻¹]	V_M [cm ³ g ⁻¹]	V_{meso}/V_{total} [%] ^[b]	Structure ^[c]
P15K-1	(70:30)	449	371	0.268	0.184	31.34	sphere
P15K-2	(65:35)	548	405	0.404	0.202	50.00	cylinder
P15K-3	(60:40)	606	416	0.537	0.207	61.45	cylinder
P15K-4	(55:45)	642	415	0.621	0.206	66.82	gyroid
P15K-5	(50:50)	446	398	0.234	0.198	15.38	lamellae
P15K-6	(45:55)	439	396	0.226	0.196	13.27	disorder

[a] S_{BET} is the total BET surface area and S_M is the micropore surface area calculated from the t-plots. [b] V_{meso} was estimated from the difference between the total pore volume and the micropore volume. [c] The pore structure was determined from SAXS and TEM characterization.

terns of the cylinder-type mesoporous carbon before (P15K-3) and after (P15K-3CA) calcination (or carbonization); the SAXS reflection signals, which suggest hexagonal packing, became stronger and clearer after removal of the template (PEO-PCL). The mesophase of the P15K-3A1 activated mesoporous carbons was also monitored through SAXS analysis (Figure 3a), with a typical hexagonally packed structure, which was revealed as $1:3^{1/2}:7^{1/2}$, confirming that the pore structure remained after KOH activation at 800 °C. Figure 3b and c presents TEM images of the mesoporous carbons before activation; the top- and side-view images are consistent with a hexagonal cylinder structure. TEM images of the P15K-3A1 activated mesoporous carbon are presented in Figure 3d and e, again revealing a hexagonal cylinder structure in the top (001) and side views, respectively, and were consistent with the results of the SAXS analysis. We observed similar phenomena for the gyroid-type mesoporous carbons. In the SAXS patterns (Figure 4a), the gyroid characteristics were clearer after calcination (P15K-4 and P15K-4CA), and the mesophase was retained perfectly after activation with KOH (P15K-4A1). The classic hexagonally packed face (111) of the gyroid structure was present both before (Figure 4b) and after (Figure 4d) activation. Another typical face of the gyroid structure (311) is evident in Figure 4c (before activation, P15K-4CA) and e (after activation, P15K-4A1), implying that the structure remained ordered even after KOH activation. Table 2 presents the textural properties of the mesoporous carbon samples (cylinder P15K-3CA and gyroid P15K-4CA) and activated mesoporous carbon samples (cylinder P15K-3A1 and gyroid P15K-4A1). The pore sizes of the mesoporous carbons increased after activation for both the cylinder (from 12.3 to 15.6 nm, Figure 5b) and gyroid (from 12.2 to 14.1 nm, Figure 5d) structures.

On the other hand, the BET surface areas of the mesoporous carbons were enhanced dramatically after KOH activation, suggesting that the KOH activation process not only created new micropores but also increased the sizes of the larger mesopores. These surface areas and pore sizes were higher than those reported from other previous studies of mesoporous carbons.^[33–37] The hysteresis loops of the mesoporous carbon samples and the activated mesoporous carbon samples had similar shapes (Figures 5a and c), implying that the pore structures were retained after activation with KOH. The hysteresis loops of those carbon materials were consistent with typical mesoporous materials and H_1 -like cylindrical pores. To further investigate the mesoporous carbon structures after KOH activation, we recorded Raman spectra to explore the intrinsic properties

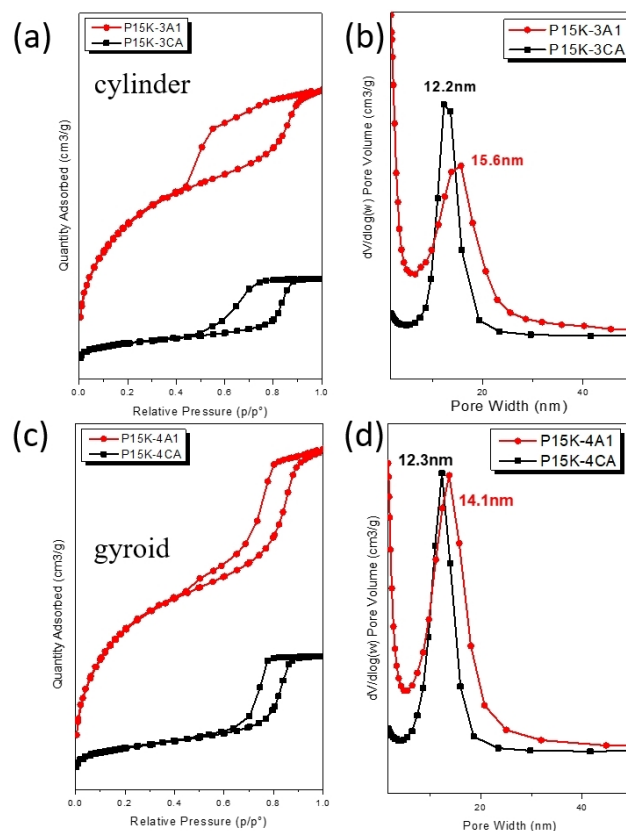


Figure 5. (a, c) N_2 adsorption/desorption isotherms and (b, d) pore size distribution curves of the cylinder-like mesoporous carbon P15K-3 and gyroid-like mesoporous carbon P15K-4 before (P15K-3CA and P15K-4CA) and after (P15K-3A1 and P15K-4A1) activation.

of the carbon materials during the process of KOH activation. We determined the degree of graphitization roughly from the I_D/I_G ratio, where the G band represents the vibrations of sp^2 hybridized orbitals of carbon-carbon bonds. Figure 6a and b presents the Raman spectra of the cylinder- and gyroid-like mesoporous carbons P15K-3CA and P15K-4 CA, respectively; the value of I_D/I_G increased from 1.10 to 1.13 for the cylinder-type mesoporous carbon and from 1.07 to 1.10 for the mesoporous carbon with the gyroid pore structure, implying that the planar structures of the carbon materials were slightly destroyed during the process of KOH activation (red curves provide the Raman spectra of the activated mesoporous carbons). In other words, we expected the activated mesoporous carbons to retain a certain degree of conductivity suitable for use as electrode materials.

Table 2. Textural properties of the mesoporous carbon samples P15K-3CA, P15K-3A1, P15K-4CA, and P15K-4A1.

Sample	Pore size [nm] ^[a]	S_{BET} [$m^2 g^{-1}$] ^[a]	S_M [$m^2 g^{-1}$] ^[a]	V_{total} [$cm^3 g^{-1}$]	V_M [$cm^3 g^{-1}$]	V_{meso}/V_{total} [%] ^[b]	I_D/I_G ^[c]	Structure
P15K-3CA	12.3	642	415	0.62	0.21	67	1.1	cylinder
P15K-3A1	15.6	1865	390	1.37	0.21	85	1.3	cylinder
P15K-4CA	12.2	606	416	0.54	0.21	61	1.07	gyroid
P15K-4A1	14.1	1920	534	1.50	0.28	81	1.1	gyroid

[a] The pore size was calculated by using the BJH method, from the adsorption branch; S_{BET} is the total BET surface area and S_M is the micropore surface area calculated from the t-plots. [b] V_{meso} was estimated from the difference between the total pore volume and the micropore volume. [c] I_D and I_G are the intensities of the D- and G-bands, respectively, in the Raman spectra.

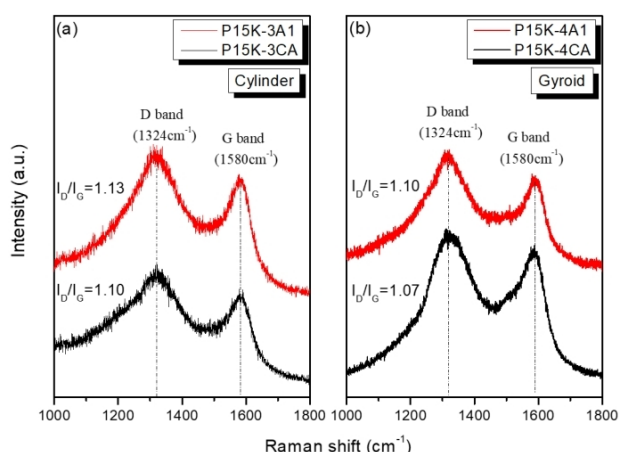


Figure 6. Raman spectra of mesoporous carbons and activated mesoporous carbons with (a) cylinder (P15K-3CA and P15K-3A1) and (b) gyroid (P15K-4CA and P15K-4A1) structures.

The activated mesoporous carbons (gyroid and cylinder structures) featured BET surface areas of approximately $2000 \text{ m}^2 \text{ g}^{-1}$, but did not undergo structural collapse, after activation, implying that they would be suitable candidates for use as electrode materials for EDLC supercapacitors. We tested the electrochemical properties of the activated mesoporous carbons P15K-3A1 and P15K-4A1 within both three-electrode cell and CR2032 coin-cell systems. Figure 7a presents the CV

scan curves recorded at a scan rate of 5 mVs^{-1} . The CV curves of the gyroid- and cylinder-type activated mesoporous carbons were of rectangular shape, indicating the typical electrical double-layer behavior of EDLC supercapacitors. Furthermore, the larger loop for the gyroid structure implies that the activated mesoporous carbon with the gyroid-type pore structure also had a specific capacitance greater than that of the cylinder-like counterpart in the $\text{KOH}_{(\text{aq})}$ electrolyte system, possibly because of the bi-continuous mesochannels in the gyroid structure. Figure 7c and d displays the galvanostatic charge/discharge curves of P15K-3A1 and P15K-4A1 at specific current densities. The symmetric charge/discharge curves indicate that the energy storage process did not involve a chemical reaction, but rather only electrostatic adsorption. Figure 7b compares the specific capacitances of the gyroid and cylinder electrode materials measured at various current densities (0.5, 1, 2, 3, and 5 Ag^{-1}). The specific capacitance of the activated mesoporous carbon P15K-3A1 at 0.5 Ag^{-1} was 155 Fg^{-1} , significantly larger than the value of 135 Fg^{-1} for the cylinder-type activated mesoporous carbon P15K-4A1. The specific capacitances decreased slightly upon increasing the current density for both electrode materials from 0.5 to 5 Ag^{-1} (Figure 7b): it decreased from 155 Fg^{-1} to approximately 145 Fg^{-1} for P15K-3A1 and from 135 Fg^{-1} to approximately 125 Fg^{-1} for P15K-4A1, suggesting that these supercapacitors were rather stable, with nearly no decay occurring at a faster charging rate.

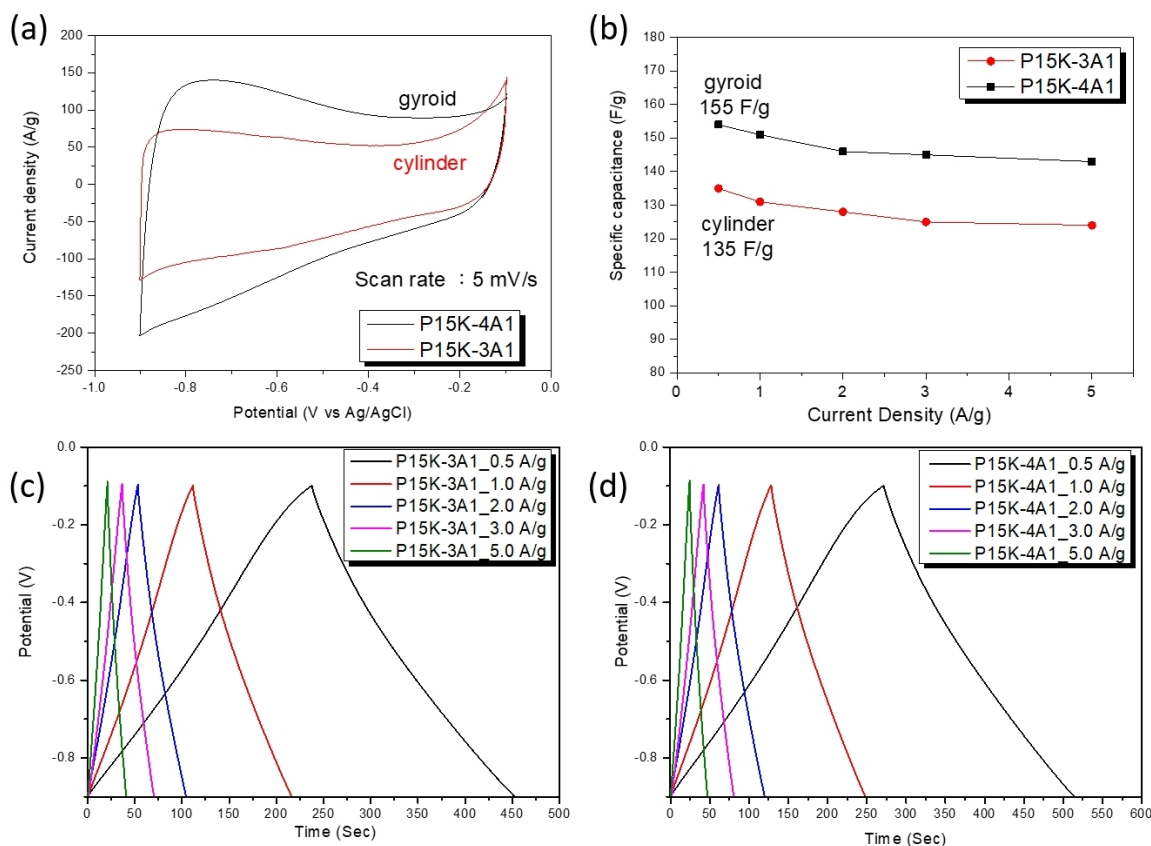


Figure 7. Electrochemical performance of the activated mesoporous carbon samples P15K-3A1 (cylinder) and P15K-4A1 (gyroid) in a three-electrode cell: (a) CV curves (scan rate: 5 mVs^{-1}); (b) galvanostatic discharge capacitances measured at current densities of 0.5, 1, 2, 3, and 5 Ag^{-1} ; and (c, d) galvanostatic charge/discharge curves of P15K-3A1 (cylinder) and P15K-4A1 (gyroid) recorded at various current densities.

To further examine the electrochemical properties of the activated mesoporous carbons as potential electrode materials for EDLC supercapacitors, we mixed the porous carbons with conductive additives and a binder into homogeneous slurries and then fabricated the electrodes assembled with bottoms, separators, spacers, springs, and tops to form CR2032 coin-cell EDLC supercapacitors. The electrolyte used here was TEABF_4 in MeCN, a common and commercialized electrolyte for commercial supercapacitors, to allow comparisons with market devices.

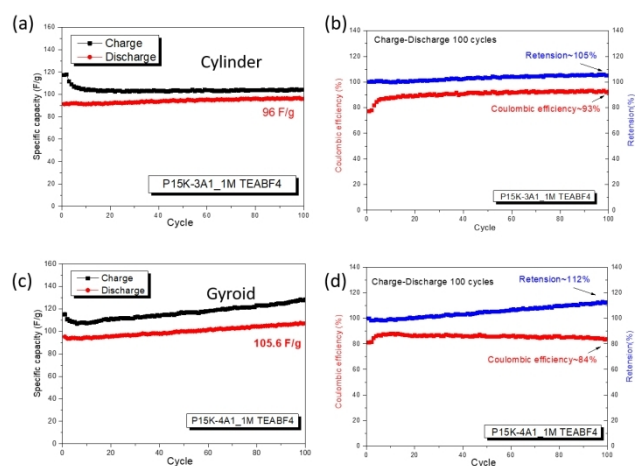


Figure 8. Cycle performance of activated mesoporous carbon samples in a two-electrode CR2032 coin-cell system in 1 M TEABF_4 at a current density of 1.0 Ag^{-1} : (a, c) galvanostatic charge/discharge curves of (a) the cylinder-type mesoporous carbon sample P15K-3A1 and (c) the gyroid-type sample P15K-4A1; (b, d) coulombic efficiency and retention curves of (b) P15K-3A1 and (d) P15K-4A1.

Figure 8 presents the electrochemical performance of P15K-3A1 (cylinder) and P15K-4A1 (gyroid) as electrode materials; Figure 8a and c displays the charge/discharge performances (100 cycles) of the cylinder and gyroid electrode materials. The stable capacitance of the cylinder-type electrode material was approximately 96 F g^{-1} , and its charge/discharge curve was rather smooth. Although the specific capacitance of the gyroid-type porous carbon material (ca. 105.6 F g^{-1}) was significantly higher, its charge/discharge behavior was not stable after 100 cycles; the charge and discharge capacitances both kept rising, possibly because the electrolyte did not reach stable diffusion conditions or because the actual specific capacitance of the gyroid-like carbon material was probably

higher after equilibration. Similar phenomena were evident in the retention and coulombic efficiency curves (Figure 8b and d). The retention of the cylinder-like carbon increased slightly to 105%, and its coulombic efficiency was approximately 93%. For the gyroid carbon sample, the capacitance was enhanced (retention: ca. 112%) and the coulombic efficiency was relatively low (ca. 84%), possibly because of the conditions of the coin-cell. Table 3 summarizes the electrochemical performances of the cylinder-like carbon P15K-3A1 and the gyroid-like carbon P15K-4A1. The specific capacitance of the gyroid carbon sample (P15K-4A1) was higher in both $\text{KOH}_{(\text{aq})}$ and $\text{TEABF}_4/\text{MeCN}$ systems, presumably a benefit of its bi-continuous pore structure, implying that this kind of carbon structure might be more suitable as a candidate electrode material for EDLC supercapacitors. In addition, the cycling stability performance of gyroid and cylinder carbon was also tested at 10.0 Ag^{-1} within a very wide potential range (-1.0 up to 1.0 V) in 6.0 M KOH (Figure S1 in the Supporting Information). The cycling capability showed an extraordinary stable performance with an average coulombic efficiency of 99% for gyroid carbon and 98% for cylinder carbon. This performance is considered an extremely stable presentation of capacitance retention for both materials. It is interesting to compare the difference between the ionic liquid's stability with the aqueous medium, which provided an easy diffusion and further excellent stability with coulombic efficiencies.

To study the diffusion, the electrochemical impedance spectra were also studied. The charge transfer rates were tested through electrochemical impedance spectroscopy (EIS). The EIS curves (Figure S2 in the Supporting Information) of the gyroid and cylinder materials on indium tin oxide (ITO) glass were investigated within the frequency range 100 mHz to 100 kHz at the open circuit potential and 5 mV as an amplitude. The impedance plot showed a well-designed Warburg diffusion combined with solution and charge transfer resistance. Therefore, the simulated equivalent circuit matches with the Randles cell, which is composed of four elements; the solution resistance (R_s), the charge-transfer resistance (R_{ct}), the electrical double-layer capacitance (C_{dl}), and Warburg diffusion impedance (W_d), as displayed in the inset of Figure S2 and Table S1 (in the Supporting Information). Both materials matched with the Randles circuit analysis models with more favorable diffusion for gyroid carbon compared with the cylinder carbon. It is possible that the pores in gyroid carbon was better matched with the aqueous electrolyte than the pores in the cylinder. All of the per-

Table 3. Textural properties and electrochemical capacitances of P15K-3A1 (cylindrical structure) and P15K-4A1 (gyroid structure).

Sample	S_{BET} [$\text{m}^2 \text{ g}^{-1}$]	Pore size [nm] ^[a]	V_{total} [$\text{cm}^3 \text{ g}^{-1}$]	V_{micro} [$\text{cm}^3 \text{ g}^{-1}$]	Structure	Capacitance ^[b] (6 M KOH) [F g^{-1}]	Capacitance ^[c] (1 M TEABF_4) after 100 cycles [F g^{-1}]
P15K-3A1	1865	14.1	1.367	0.205	cylinder	135	96
P15K-4A1	1920	15.6	1.500	0.278	gyroid	155	105.6

[a] The pore size was calculated by using the BJH method, from the adsorption branch. [b] The aqueous capacitances were calculated in a three-electrode cell under 6 M $\text{KOH}_{(\text{aq})}$ at a current density of 0.5 Ag^{-1} . [c] The organic capacitances were calculated in a two-electrode CR2032 coin-cell system under 1 M $\text{TEABF}_4/\text{MeCN}$.

formance data are good when compared with those from other previous studies of EDLC supercapacitors incorporating mesoporous carbon^[33–40] and nonporous carbons (Table S2 and References S1–S12 in the Supporting Information).

Conclusion

We have prepared a series of mesoporous carbons by using PEO-PCL as the template to give cylinder and gyroid pore structures. The surface areas of these mesoporous carbons were further increased to approximately 2000 m²g⁻¹ without collapse of the pore structures. The resulting activated mesoporous carbon samples (cylinders and gyroids) were applied as electrode materials for EDLC supercapacitors. The electrochemical properties of the activated mesoporous carbons were tested by using a three-electrode system (KOH_(aq)) and a CR2032 coin-cell system (commercialized electrolyte, TEABF₄/MeCN). The cylinder-type carbon sample provided specific capacitances of 135 Fg⁻¹ in 6 M KOH_(aq) and 96 Fg⁻¹ in 1 M TEABF₄/MeCN; for the gyroid carbon sample, these values were 155 and 105.6 Fg⁻¹, respectively. The interconnected mesopores of the gyroid-type porous carbon sample were responsible for the superior capacities during charge/discharge experiments, presumably because of its more efficient transport channels and greater effective surface area for ion adsorption. The larger and interconnected mesopores of the electrode materials would presumably make them suitable electrode materials for ionic liquid electrolyte systems, potentially providing EDLC supercapacitors with even higher energy densities. The porous carbons could provide higher surface area for the storage of ions (higher capacity and energy), in addition, the mesoporous structure is expected to be helpful for electrolyte transportation.

Acknowledgments

This study was supported financially by the Ministry of Science and Technology, Taiwan, under contracts MOST 105-2221-E-110-092-MY3 and 106-2221-E-110-067-MY3.

Conflict of interest

The authors declare no conflict of interest.

Keywords: bi-continuous gyroid structures · block copolymers · mesoporous carbon · supercapacitors

- [1] D. R. Dekel, *J. Power Sources* **2018**, *375*, 158–169.
- [2] V. Yarlagadda, M. K. Carpenter, T. E. Moylan, R. S. Kukreja, R. Koestner, W. Gu, L. Thompson, A. Kongkanand, *ACS Energy Lett.* **2018**, *3*, 618–621.
- [3] Y. Q. Liang, Y. J. Wang, C. Mu, S. Wang, X. N. Wang, D. S. Xu, L. C. Sun, *Adv. Energy Mater.* **2018**, *8*, 1701159.
- [4] C. Sun, F. Pan, H. Bin, L. Xue, B. Qiu, Z. Wei, Z. G. Zhang, Y. Li, *Nat. Commun.* **2018**, *9*, 743.
- [5] K. Al-Attafi, A. Nattestad, Q. Wu, Y. Ide, Y. Yamauchi, S. X. Dou, J. H. Kim, *Chem. Commun.* **2018**, *54*, 381–384.

- [6] S. Logeshkumar, R. Manoharan, *Electrochim. Acta* **2014**, *144*, 147–153.
- [7] L. A. Yolshina, V. A. Yolshina, A. N. Yolshin, S. V. Plaksin, *J. Power Sources* **2015**, *278*, 87–97.
- [8] S. Gao, Y. T. Cheng, M. Shirpour, *ACS Appl. Mater. Interfaces* **2019**, *11*, 982–989.
- [9] J. H. Lu, F. Lian, L. L. Guan, Y. X. Zhang, *J. Mater. Chem. A* **2019**, *7*, 991–997.
- [10] G. Xu, L. Ding, T. Wu, M. Xiang, F. Yang, *J. Polym. Res.* **2018**, *25*, 166.
- [11] A. F. M. El-Mahdy, C. H. Kuo, A. Alshehri, C. Young, Y. Yamauchi, J. Kim, S. W. Kuo, *J. Mater. Chem. A* **2018**, *6*, 19532–19541.
- [12] A. F. M. El-Mahdy, C. Young, J. Kim, J. You, Y. Yamauchi, S. W. Kuo, *ACS Appl. Mater. Interfaces* **2019**, *11*, 9343–9354.
- [13] L. Chang, K. Sun, Y. H. Hu, *ACS Appl. Mater. Interfaces* **2018**, *10*, 33162–33169.
- [14] M. Majumder, R. B. Choudhary, A. K. Thakur, *Carbon* **2019**, *142*, 650–661.
- [15] Y. Guo, Z. Q. Shi, M. M. Chen, C. Y. Wang, *J. Power Sources* **2014**, *252*, 235–243.
- [16] J. Zhi, W. Zhao, X. Y. Liu, A. R. Chen, Z. Q. Liu, F. Q. Huang, *Adv. Funct. Mater.* **2014**, *24*, 2013–2019.
- [17] A. F. M. El-Mahdy, Y. H. Hung, T. H. Mansoure, H. H. Yu, T. Chen, S. W. Kuo, *Chem. Asian. J.* **2019**, *14*, 1429–1435.
- [18] J. Li, N. Wang, J. R. Tian, W. Z. Qian, W. Chu, *Adv. Funct. Mater.* **2018**, *28*, 1806153.
- [19] M. Khandelwal, A. Kumar, *J. Mater. Chem. A* **2015**, *3*, 22975–22988.
- [20] T. Liu, B. Lee, M. J. Lee, J. Park, Z. Chen, S. Noda, S. W. Lee, *J. Mater. Chem. A* **2017**, *5*, 13511–13525.
- [21] Z. Liu, K. K. Xiao, H. Guo, X. H. Ning, A. P. Hu, Q. L. Tang, B. B. Fan, Y. F. Zhu, X. H. Chen, *Carbon* **2017**, *117*, 163–173.
- [22] Y. Y. Lv, F. Zhang, Y. Q. Dou, Y. P. Zhai, J. X. Wang, H. J. Liu, Y. Y. Xia, B. Tu, D. Y. Zhao, *J. Mater. Chem.* **2012**, *22*, 93–99.
- [23] J. Wei, D. D. Zhou, Z. K. Sun, Y. H. Deng, Y. Y. Xia, D. Y. Zhao, *Adv. Funct. Mater.* **2013**, *23*, 2322–2328.
- [24] Y. H. Deng, J. Liu, C. Liu, D. Gu, Z. K. Sun, J. Wei, J. Y. Zhang, L. J. Zhang, B. Tu, D. Zhao, *Chem. Mater.* **2008**, *20*, 7281–7286.
- [25] Y. Deng, C. Liu, D. Gu, T. Yu, B. Tu, D. Zhao, *J. Mater. Chem.* **2008**, *18*, 91–97.
- [26] W. C. Chu, B. P. Bastakoti, Y. V. Kaneti, J. G. Li, H. R. Alamri, Z. A. Allothman, Y. Yamauchi, S. W. Kuo, *Chem. Eur. J.* **2017**, *23*, 13734–13741.
- [27] J. G. Li, W. C. Chu, U. S. Jeng, S. W. Kuo, *Macromol. Chem. Phys.* **2013**, *214*, 2115–2123.
- [28] J. G. Li, C. Y. Chung, S. W. Kuo, *J. Mater. Chem.* **2012**, *22*, 18583–18595.
- [29] J. G. Li, Y. D. Lin, S. W. Kuo, *Macromolecules* **2011**, *44*, 9295–9309.
- [30] J. G. Li, C. Y. Tsai, S. W. Kuo, *Polymers* **2014**, *6*, 1794–1809.
- [31] J. G. Li, S. W. Kuo, *RSC Adv.* **2011**, *1*, 1822–1833.
- [32] M. W. Matsen, M. Schick, *Curr. Opin. Colloid Interface Sci.* **1996**, *1*, 329–326.
- [33] N. Yoshida, Y. Hirota, Y. Uchida, T. Asada, N. Kobayashi, N. Nishiyama, *Microporous Mesoporous Mater.* **2018**, *272*, 217–221.
- [34] A. Dobashi, J. Maruyama, Y. Shen, M. Nandi, H. Uyama, *Carbohydr. Polym.* **2018**, *200*, 381–390.
- [35] P. Chang, K. Matsumura, J. Zhang, J. Qi, C. Wang, T. Kinumoto, T. Tsunamura, M. Chen, M. Toyoda, *J. Mater. Chem. A* **2018**, *6*, 10331–10339.
- [36] O. Noonan, Y. Liu, X. Huang, C. Yu, *J. Mater. Chem. A* **2018**, *6*, 14272–14280.
- [37] J. Hwang, R. Yan, M. Oschatz, B. V. K. J. Schmide, *J. Mater. Chem. A* **2018**, *6*, 23521–23530.
- [38] H. Tian, S. Y. Zhu, F. G. Xu, W. T. Mao, H. Wei, Y. Y. Mai, X. L. Feng, *ACS Appl. Mater. Interfaces* **2017**, *9*, 43975–43982.
- [39] H. Tian, N. Wang, F. G. Xu, P. F. Zhang, D. Hou, Y. Y. Mai, X. L. Feng, *J. Mater. Chem. A* **2018**, *6*, 10354–10360.
- [40] Y. F. He, X. D. Zhuang, C. J. Lei, L. C. Lei, Y. Hou, Y. Y. Mai, X. L. Feng, *Nano Today* **2019**, *24*, 103–119.

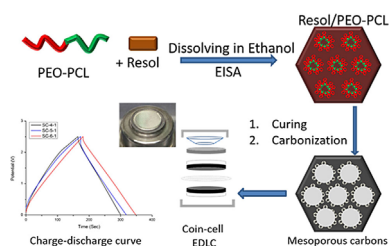
Manuscript received: April 13, 2019

Accepted manuscript online: June 17, 2019

Version of record online: ■■■■■ 0000

FULL PAPER

Activated mesoporous carbons are fabricated with pore structures with cylinder and gyroid nanostructures through the templating effect of amphiphilic poly(ethylene oxide-*block*-caprolactone) (PEO-PCL) and by using specific resol/PEO-PCL weight ratios (e.g., 60:40 for cylinders; 55:45 for gyroids). After carbonization and KOH activation, the activated mesoporous carbons were tested as electrode materials for electric double-layer capacitor (EDLC) supercapacitors.

**Mesoporous Carbons**

J.-G. Li,* Y.-F. Ho, M. M. M. Ahmed,
H.-C. Liang, S.-W. Kuo*



**Mesoporous Carbons Templated by
PEO-PCL Block Copolymers as
Electrode Materials for
Supercapacitors**

